applied sciences

MDPI

Article

Characterization of Axial Geometric Variations and Dimensional Deviation Analysis of High-Speed Ball Bearings for New Energy Vehicles Using X-Ray Computed Tomography

Yanan Zhang [1], Feng Zhang [1], Songyang Jia [1,2], Sier Deng [1], Hongjian Wu [3,*] and Jing Pang [3]

[1] School of Mechatronics Engineering, Henan University of Science and Technology, Luoyang 471003, China; zyn@haust.edu.cn (Y.Z.)
[2] Luoyang Bearing Group Co., Ltd., Luoyang 471039, China
[3] School of Agricultural Equipment Engineering, Henan University of Science and Technology, Luoyang 471003, China; pangjing@haust.edu.cn
* Correspondence: 9906245@haust.edu.cn

Abstract

As new energy vehicle drive motors develop toward higher rotational speeds and power levels, a more comprehensive characterization of the geometric condition of high-speed ball bearings is increasingly required, while conventional single-section measurements have difficulty capturing continuous axial geometric variations. To characterize continuous axial geometric variations in high-speed ball bearings for new energy vehicle drive motors and explore whether these variations exhibit trends consistent with vibration responses, four typical bearing models were investigated using X-ray computed tomography (XCT), reconstruction, and dimensional extraction. Equivalent inner and outer diameters were obtained from consecutive sections within the selected axial profile segment. The mean values of the equivalent inner and outer diameters were used to represent the dimensional level, while the standard deviation and range were used to quantify the axial fluctuations. The results showed that the equivalent inner and outer diameters of different bearing samples exhibited different degrees of axial variation within the selected axial profile segments. Meanwhile, the mean equivalent inner and outer diameters measured by XCT differed from the corresponding nominal dimensions. Further comparison showed that, within the current sample set, no stable correspondence was observed between the axial variation descriptors of the XCT-derived equivalent inner and outer diameters and the vibration test results. XCT can nondestructively acquire geometric information from consecutive axial sections and quantitatively characterize equivalent inner and outer diameter fluctuations, complementing single-section roundness measurement and providing theoretical guidance for surface-quality evaluation and manufacturing-process improvement.

Keywords: X-ray computed tomography; high-speed ball bearing; axial profile segment; axial geometric variation; equivalent diameter

Check for updates

Academic Editors: Paolo Renna and Dario Croccolo

Received: 12 August 2026
Revised: 6 October 2026
Accepted: 22 October 2026
Published: 25 October 2026

Copyright: © 2026 by the authors. Licensee MDPI, Basel, Switzerland. This article is an open access article distributed under the terms and conditions of the Creative Commons Attribution (CC BY) license.

1. Introduction

In recent years, new energy vehicles, including battery electric vehicles, plug-in hybrid electric vehicles (including range-extended electric vehicles), and fuel cell electric vehicles, have continued to develop. With the increasing demand for longer driving ranges and higher performance, electric drive systems have gradually developed toward higher rotational speeds and higher power densities [1,2]. Against this background, bearings are

required to operate under higher rotational speeds and loads, and increasing attention has been paid to their geometric condition and operational stability [3–6]. Previous studies have shown that geometric errors of rolling elements can affect the rotational accuracy of rolling bearings [7], while factors such as local raceway defects, radial clearance, load, and rotational speed can also influence the dynamic response of bearings [8,9]. The bearing bore and outer cylindrical surface are important reference surfaces for assembly and positioning. Therefore, characterizing their geometric features and comparing the geometric characterization results with the vibration test results for the same samples can be used to examine whether the static geometric condition and dynamic vibration response exhibit consistent variation trends.

According to GB/T 32324-2015, conventional roundness measurement can quantitatively characterize local profile-form deviations of a selected section [10]; however, a single-section measurement cannot readily capture continuous geometric variations across different axial positions. XCT is a nondestructive testing method that can provide cross-sectional information on the internal and external structures of an object from reconstructed data [11,12]. With advances in detector, imaging, and reconstruction technologies, its engineering applications have continued to expand [13–16]. From the perspective of geometric information acquisition and evaluation, XCT applications may involve structural visualization, quantitative dimensional characterization, and further metrological validation. Structural visualization mainly uses reconstructed images to observe internal structures and defects, whereas quantitative dimensional characterization further extracts geometric dimensions from XCT reconstruction data. When XCT is further applied to dimensional metrology, its measurement capability and the reliability of the resulting measurements need to be evaluated through measurement uncertainty, metrological structural resolution, system geometric calibration, and related assessments [17–20]. Previous studies have used XCT for the nondestructive visualization of the distribution and state of grease inside ball bearings [21]. In contrast, the present study extracts the equivalent diameters of the bearing bore and outer cylindrical surface slice by slice from consecutive XCT sections, thereby obtaining a consecutive sequence of equivalent diameters that preserves the positional order within the selected axial range and is used to characterize axial geometric variations.

Specifically, XCT was used to scan and reconstruct four types of high-speed deep-groove ball bearings for new energy vehicle drive motors, and the equivalent diameters of the bearing bore and outer cylindrical surface were extracted slice by slice from consecutive sections within the selected axial profile segment. The slice-by-slice equivalent-diameter sequences were used to preserve information on different axial positions and local variations, whereas the mean, standard deviation, and range were used to summarize the overall dimensional level and the degree of axial variation. Subsequently, the XCT results were compared with the single-section roundness measurement results to examine the complementary information provided by the two geometric characterization methods. The XCT mean equivalent inner and outer diameters were compared with the corresponding nominal dimensions to describe the numerical differences between the current measurements and the nominal dimensions. In addition, the axial geometric variation descriptors were exploratorily compared with the vibration test results of the same samples to examine whether the two types of results exhibited consistent variation trends. Therefore, this study primarily uses consecutive XCT sections to obtain continuous axial geometric information on the bearing bore and outer cylindrical surface and further analyzes the variation characteristics revealed by different geometric characterization results and their comparison with the vibration test results.

2. Materials and Methods

2.1. Test Equipment

XCT scanning of the high-speed ball bearings for new energy vehicles was performed using a three-dimensional X-ray microscope (nanoVoxel3000, Tianjin Sanying Precision Instruments Co., Ltd., Tianjin, China). The equipment mainly consists of an X-ray source, a rotary stage, a detector, a mechanical system, a computer system, and a radiation-shielding enclosure, as shown in Figure 1. Figure 1a shows the overall appearance of the equipment, Figure 1b shows its key internal components, and Figure 1c presents a schematic diagram of the imaging principle. The equipment can accommodate samples with a maximum diameter of 300 mm and a maximum height of 250 mm and supports multiple scanning modes, including digital radiography (DR), CT scanning, and SQ helical scanning. The maximum tube voltage is 190 kV, the highest resolution is 2 μm, the imaging area of the high-sensitivity flat-panel detector is 300 mm × 250 mm, and the detector pixel size is 100 μm.

After scanning, image reconstruction was performed using Voxelstudio Recon (Version 2.5.1.25), and the reconstructed images were analyzed and geometrically measured using Dragonfly (Version 2024.1).

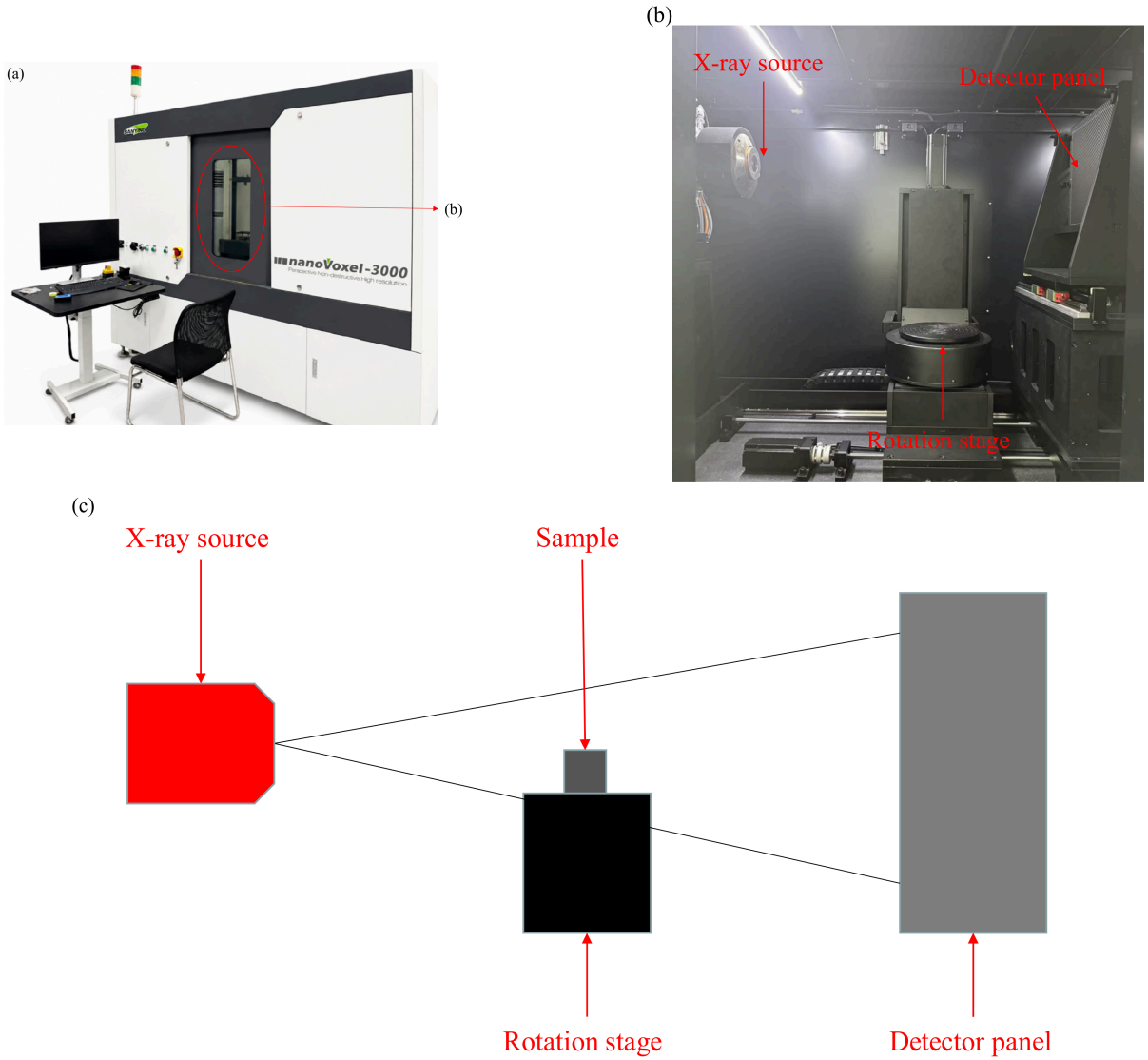


Figure 1. Three-dimensional X-ray microscope: (**a**) overall appearance of the equipment; (**b**) key internal components; (**c**) schematic diagram of the imaging principle.

For the measurement of the roundness errors of selected sections of the bearing bore and outer surface, a roundness measuring instrument (RA143C-awe, Shaanxi Will Electromechanical Technology Co., Ltd., Xi'an, China) was used, as shown in Figure 2. The instrument uses a precision rotary spindle as the measurement datum. An inductive sensor is used to collect the radial displacement signal of the measured profile relative to the spindle rotation datum, and the data are processed by the computer system. The instrument mainly consists of a rotating worktable, vertical axis, horizontal arm, inductive sensor, and computer data processing system. The instrument has a total weight of 260 kg and overall dimensions of 1300 mm × 700 mm × 1750 mm. Its rated voltage and rated power are 220 V and 500 W, respectively.

For the measurement of the bearing vibration acceleration level and vibration velocities in the low-, medium-, and high-frequency bands, a bearing vibration measuring instrument (S0910C, Luoyang Bearing Research Institute Co., Ltd., Luoyang, China) was used, as shown in Figure 3. During the test, the bearing was mounted on a mandrel matching its model, and the inner ring was driven to rotate by the drive unit. The vibration sensor was placed in contact with the middle of the width of the outer cylindrical surface of the outer ring to collect vibration signals during bearing operation. After the signals were processed by the preamplifier circuit and computer system, parameters including vibration acceleration and vibration velocity were obtained. The instrument is suitable for bearings with bore diameters of Φ10–Φ60 mm. The measurement ranges for vibration acceleration and vibration velocity are 10–90 dB and 0–8000 μm/s, respectively. The spindle speed was set to 1800 r/min. The amplitude linearity error is no greater than 3%, and the system calibration error is no greater than 0.5 dB.

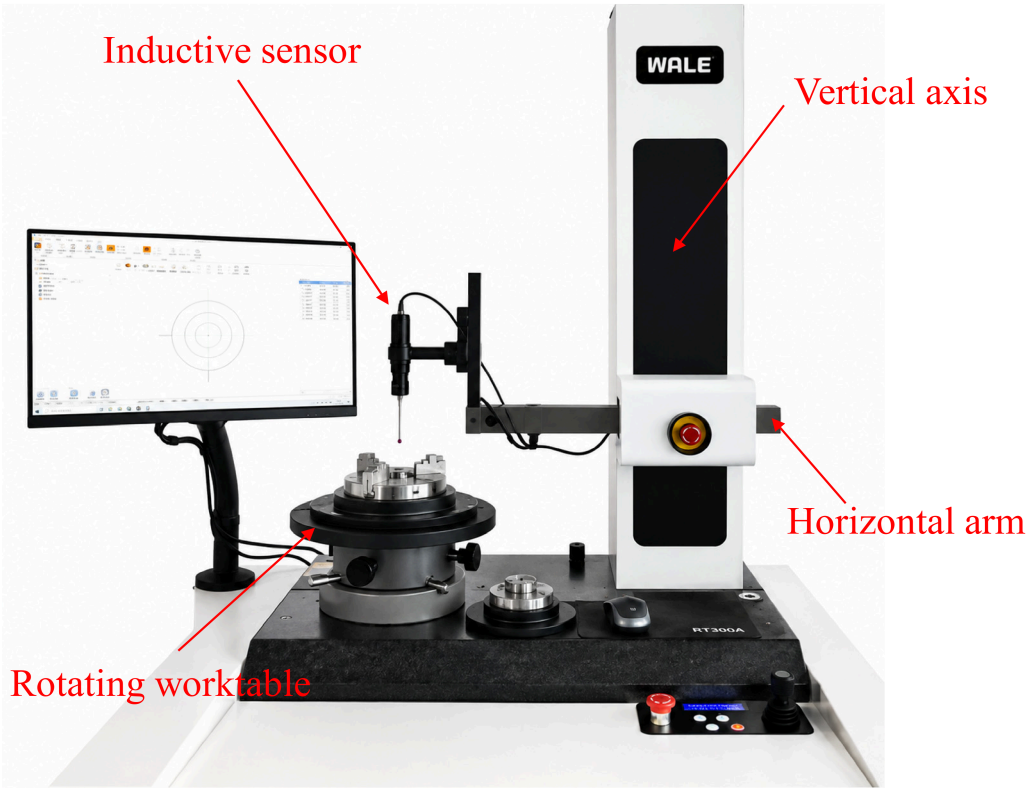


Figure 2. Appearance of the RA143C-awe roundness measuring instrument.

2.2. Test Bearings

Four typical types of high-speed deep groove ball bearings (CW Bearing, Ningbo Cixing Bearing Co., Ltd., Ningbo, China) for new energy vehicle drive motors were selected

in this study: 6207, 6208, 6306, and 6307. These four bearing types are denoted as A, B, C, and D, respectively, with three bearing samples selected for each type. No specific statistical sampling method was employed for selecting the three samples of each bearing type. Owing to their simple structure and high radial load-carrying capacity, these bearings are widely used in electric drive systems for new energy vehicles, and their vibration characteristics directly affect the operational stability of the equipment. To compare the static geometric information and the vibration response of the same sample under specified operating conditions, XCT geometric measurement, roundness measurement, and vibration testing were each performed once on all 12 bearing samples. The XCT axial geometric characterization parameters were then matched with the vibration characteristic parameters for the corresponding samples to examine whether the two types of parameters exhibited consistent variation trends [22,23]. The main structural and dimensional parameters of the test bearings are listed in Table 1.



Figure 3. S0910C bearing vibration measuring instrument manufactured by Luoyang Bearing Research Institute Co., Ltd.

Table 1. Main structural and dimensional parameters of the bearings.

Code	Inner Diameter (mm)	Outer Diameter (mm)	Width (mm)	Number of Rolling Elements	Rolling Element Diameter (mm)	Pitch Diameter (mm)	Contact Angle (°)
A	35	72	17	9	11.112	53.5	0
B	40	80	18	9	11.906	60	0
C	30	72	19	8	12.7	53.5	0
D	35	80	21	7	15.875	59	0

2.3. Test Methods

2.3.1. XCT Scanning, Reconstruction, and Geometric Measurement

To characterize the geometric information of the high-speed ball bearings for new energy vehicles, XCT scans were performed on the 12 bearing samples described above. Before scanning, the three-dimensional X-ray microscope was preheated to ensure stable operation of the X-ray source, and the maximum scanning voltage was set according to the material type. The maximum scanning voltage of the equipment is 190 kV, and the voltage used for the formal scan should not exceed this value. The bearing samples were fixed on the rotating stage, and position calibration was performed to reduce the effect of positional deviations during scanning on the reconstruction results. The main position calibration parameters included the X-axis position of the rotating stage, X_1, the Z-axis position of the rotating stage, Z_1, and the X-axis position of the detector, X_2. X_1 represents the horizontal position of the rotary stage and is used to determine the horizontal scanning position of the sample; Z_1 represents the vertical position of the rotary stage and is used to adjust the scanning height of the sample; and X_2 represents the horizontal position of the detector and is used to determine the position of the detector relative to the sample and the X-ray source. Together, these parameters are used for position calibration before scanning to establish a scanning geometry suitable for the current bearing sample.

A pre-scan was performed before the formal scan to determine appropriate scanning conditions for the bearing samples. Based on the pre-scan results, the tube voltage, exposure time, and filtering conditions were adjusted [24]. The tube voltage for the formal scan was ultimately set to 185 kV, with a 1 mm Cu filter and an exposure time of 2.8 s. The measured penetration rate during the formal scan was 18.151%, which falls within the recommended range of 10–20% reported in the relevant literature and provides appropriate grayscale contrast for subsequent image reconstruction and contour extraction [25].

The spatial resolving capability of XCT reflects the ability of the system to distinguish internal details of the sample. The effective pixel size at the sample plane is jointly determined by the detector pixel size and the geometric magnification of the system. The system used in this study adopts a geometric magnification imaging mode. The pixel size of the images obtained in this scan was calculated as follows:

$$P = d\frac{SOD}{SDD} \tag{1}$$

where P is the pixel size at the sample plane, SOD is the source-to-object distance, SDD is the source-to-detector distance, and d is the detector pixel size, which is 100 μm for the system used in this study.

During the position calibration described above, the X_1 and Z_1 positions of the rotating stage were set to 580 mm and 235 mm, respectively, and the X_2 position of the detector was set to 550 mm. The equipment software showed an SOD of 169.41 mm and an SDD of 452.94 mm. According to Equation (1), the corresponding pixel size was calculated to be 37.4 μm. Subsequently, based on the scanning voltage and power, the current was set to 135 μA to ensure stable operation of the X-ray source and improve the imaging quality. After the pixel size and penetration rate met the test requirements, the field of view of the sample was calibrated, and a two-dimensional reference image was obtained by a rapid DR scan to provide a correction reference for the formal CT scan, thereby ensuring the accuracy of subsequent three-dimensional reconstruction and the reliability of the measurements.

In summary, the complete parameter settings used for XCT scanning are listed in Table 2. The rotating stage positions X_1 and Z_1 were set to 580 mm and 235 mm, respectively, and the detector position X_2 was set to 550 mm. The scanning voltage was 185 kV, the current was 135 μA, the exposure time was 2.8 s, the pixel size at the sample plane was

37.4 μm, and a 1 mm copper filter was used. During scanning, artifact removal was enabled to reduce the influence of metal artifacts on profile visualization. Meanwhile, self-compression was enabled to reduce memory usage, and the acquisition frame count was set to 1440 FPS.

Table 2. XCT scanning parameters for the bearings under test.

Parameter Name	Parameter Values
Horizontal position of rotating stage (X_1)	580 mm
Vertical position of rotating stage (Z_1)	235 mm
Horizontal position of detector (X_2)	550 mm
Preheating voltage	190 kV
Target voltage	185 kV
Target current	135 μA
Exposure time	2.8 s
Pixel size at the sample plane	37.4 μm
Copper filter	1 mm
Artifact removal	open
Self-compression	open
Acquisition frame rate	1440 FPS

After XCT scanning, the scanned files were imported into the post-processing software Voxelstudio Recon (Version 2.5.1.25). To reduce the influence of geometric deviations of the scanning system on the reconstruction results, the geometric parameters of the system were corrected. The geometric correction parameters commonly used in Voxelstudio Recon (Version 2.5.1.25) include the detector horizontal offset *hu*, detector vertical offset *hv*, detector angular deflection parameters *beta*, *chp*, and *theta*, and the distance from the X-ray source to the detector center (*SDD*). Among them, *hu* and *hv* are used to correct the positional deviations of the detector center in the horizontal and vertical directions, respectively, while *beta*, *chp*, and *theta* are used to describe the angular deflections of the detector in different directions. *SDD* is an important parameter that determines the geometric accuracy of reconstruction and the magnification relationship. Based on the geometric parameter correction ranges listed in Table 3, which were provided by the equipment manufacturer based on engineering experience, the above geometric parameters were adjusted using a stepwise refinement approach. During the adjustment process, the current parameter adjustment range was divided into 10 intervals, and a more appropriate parameter interval was selected by comparing the contour integrity, boundary clarity, and artifacts of the reconstructed slices under different parameter settings. The selected interval was then further subdivided and compared, and the parameter adjustment range was progressively narrowed until further adjustment no longer resulted in distinguishable changes in the reconstructed images. For different bearing samples, the geometric parameter combination suitable for each sample was individually determined using the above stepwise refinement approach within the reference ranges and was then used for subsequent image reconstruction.

After geometric correction and image reconstruction, the reconstruction results were imported into the three-dimensional image analysis software Dragonfly (Version 2024.1). Spatial parameters, including the reconstructed pixel size and the spacing between adjacent slices, were entered to generate consecutive two-dimensional slices and a three-dimensional model of the bearing. In each two-dimensional slice, three feature points at different positions along the boundary were selected, and a circle was fitted using three-point circle fitting. The diameter of the fitted circle was taken as the equivalent inner diameter (or equivalent outer diameter) of the bearing. To standardize the measurement region and reduce the influence of end fillets and edge regions on the measurement results, consec-

utive two-dimensional slices accounting for approximately 10% of the total number of reconstructed slices were selected around the middle cross-section along the axial direction of the bearing to form an axial profile segment.

Based on the statistical results of the equivalent inner and outer diameters obtained from the axial profile segment, the mean equivalent inner diameter and mean equivalent outer diameter were further compared with their corresponding nominal dimensions, respectively, and the absolute and relative deviations of the 12 bearings were calculated. The absolute deviation was calculated as the absolute value of the difference between the mean equivalent diameter measured by XCT and the corresponding nominal dimension, i.e., $|X_{XCT} - X_0|$. The relative deviation was calculated as the ratio of the absolute deviation to the corresponding nominal dimension and expressed as a percentage, i.e., $|X_{XCT} - X_0|/X_0 \times 100\%$, where X_{XCT} is the mean equivalent diameter measured by XCT, and X_0 is the corresponding nominal dimension of the bearing.

Table 3. Geometric parameter correction ranges.

Parameter	Meaning	Reference Range
hu	Detector horizontal offset	±50 pixels
beta	Detector angular offset 1	±1°
hv	Detector vertical offset	±50 pixels
chp	Detector angular offset 2	±1°
theta	Detector angular offset 3	±1°
SDD	Distance from the X-ray source focal spot to the detector center	Preset value ± 20 mm

2.3.2. Roundness Measurement and Vibration Data Analysis Methods

To obtain the roundness errors of the selected cross-sections of the bearing bore and outer surface, a conventional two-dimensional roundness measurement method was used. Figure 4 shows a schematic diagram of the minimum zone circle method. The dashed line represents the reference circle, while the solid line represents the measured cross-sectional profile. The roundness error ΔZ is defined as the difference between the maximum and minimum radii of the profile.

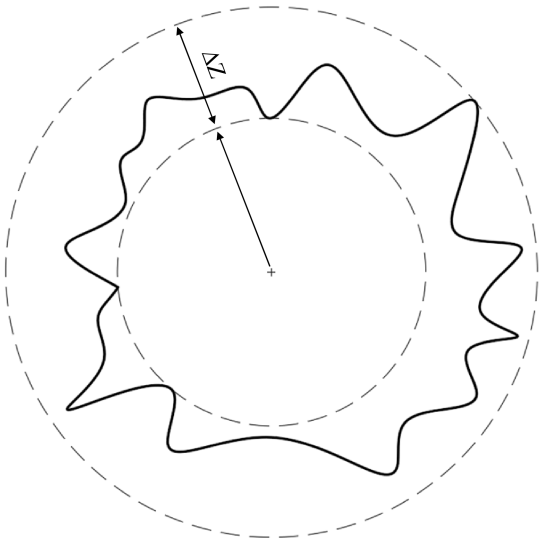


Figure 4. Schematic diagram of the minimum zone circle method. The dashed line represents the reference circle, and the solid line represents the measured cross-sectional profile.

Using the above measurement method, the roundness of the inner and outer mounting surfaces of the bearings was measured using the RA143C-awe roundness measuring instrument. The bearing to be measured was placed on the precision rotating worktable, and the position of the workpiece was finely adjusted using the mechanical centering and leveling knobs. Changes in the sensor reading were monitored in real time so that the central axis of the measured cross-section of the inner-ring bore or the outer-ring outer surface coincided with the rotational center of the instrument spindle, thereby reducing the influence of mounting eccentricity on the measurement results. A contact scanning method was used, with the stylus contacting the bore wall and the outer cylindrical surface of the bearing under a constant small measuring force. As the spindle drove the bearing through a 360° rotation, the high-sensitivity inductive sensor recorded the radial displacement signals of the surface profile relative to the rotational reference in real time, and the signals were synchronously stored in the computer system through an A/D converter. The profile data of the measured bearing cross-section were then obtained and used to calculate the single-section roundness error.

The vibration test was conducted using the S0910C bearing vibration measuring instrument described in Section 2.1. During the test, the bearing was mounted on a mandrel matched to its model, and the inner ring was rotated by the drive unit while a load was applied to the outer ring by the loading device. The vibration sensor was brought into contact with the middle of the width of the outer cylindrical surface of the outer ring to acquire vibration signals during bearing operation. The vibration acceleration level and the vibration velocities in the low-, medium-, and high-frequency bands were obtained. For each indicator, the larger of the values measured on the two sides of the bearing was used. According to the factory vibration quality requirements provided by the bearing manufacturer, the bearings were evaluated based on the V3 group requirements specified in GB/T 32325-2015 *Rolling bearings—Specifications for vibration (velocity) of deep groove ball bearings* [26]. The limits for the low-, medium-, and high-frequency bands were 120 μm/s, 60 μm/s, and 95 μm/s, respectively. If the measured value in any frequency band exceeded the corresponding limit, the bearing was considered not to meet the V3 group requirements. The vibration acceleration level was used only as a supplementary indicator. The vibration test results were matched with the XCT geometric characterization results according to the sample numbers to examine whether the two types of indicators showed consistent variation trends.

3. Results

To evaluate the proposed method for characterizing fluctuations in the equivalent inner and outer diameters based on the axial profile segment of the bearing, the XCT reconstruction results, equivalent inner and outer diameters and their axial fluctuations, single-section roundness errors, and deviations from the nominal dimensions of the 12 deep groove ball bearings were analyzed. The vibration test results were then combined with the geometric characterization results to analyze the correspondence between the static geometric characterization results and the dynamic operating state of the bearings.

3.1. XCT Reconstruction Results

To visually illustrate the influence of geometric parameter correction on reconstruction quality, reconstructed images of the same bearing under the same scanning conditions were selected for comparison. The comparison mainly focused on boundary clarity, the visualization of the inner and outer rings, and changes in metal artifacts, as shown in Figure 5.

In Figure 5, panels (a) and (b) show the reconstruction results before and after geometric parameter correction, respectively, while panels (c) and (d) show locally enlarged

views of the corresponding regions. Compared with the result before correction, the profile boundaries of the inner and outer rings are clearer after correction, and this difference is more evident in the locally enlarged regions (c) and (d). The reconstruction results obtained after geometric parameter correction were used for all subsequent contour extraction and geometric dimensional analysis.

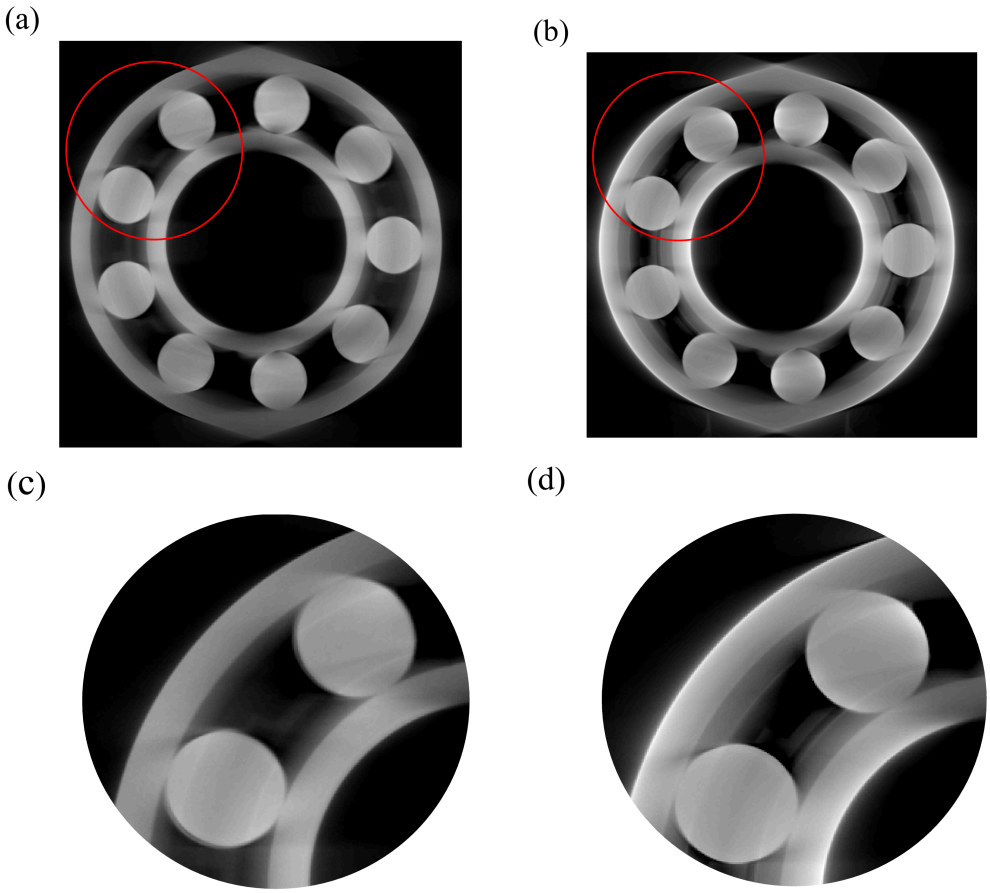


Figure 5. Comparison of reconstructed images before and after geometric parameter correction: (**a**) image before correction; (**b**) image after correction; (**c**) local enlarged view before correction; (**d**) local enlarged view after correction.

To this end, the four types of high-speed ball bearings for new energy vehicles described above were scanned and reconstructed using the scanning and reconstruction parameter settings described above, as shown in Figure 6.

In Figure 6, each row represents one group of bearing samples. From top to bottom, the four rows correspond to Groups A, B, C, and D, respectively. From left to right, the images show Samples 1, 2, and 3 of each group, followed by the corresponding photograph of the bearing. All scans were performed at a voltage of 185 kV, a current of 135 μA, an exposure time of 2.8 s, and a pixel size at the sample plane of 37.4 μm, with a 1 mm copper filter and an acquisition frame rate of 1440 FPS. XCT scanning clearly revealed the main structures of the bearings, including the inner ring, outer ring, and rolling elements. Because the cage material has a lower X-ray attenuation capability than the metallic rings and rolling elements, the cage profile appeared relatively blurred in the reconstructed images. Overall, blurred boundaries and stripe-like artifacts were still present in some regions, which may be affected by metal artifacts, resolution, and interface clarity. The reconstructed images were sufficient for identifying the bore and outer-surface profiles and for subsequent measurement of the equivalent inner and outer diameters; however, there were still certain limitations in identifying fine internal structures and small local features.



Figure 6. XCT reconstruction results and photographs of the four bearing models: (**A**) Group A; (**B**) Group B; (**C**) Group C; (**D**) Group D. For each group, the first three images show the XCT reconstruction results for Samples 1–3, respectively, and the fourth image shows the corresponding bearing photograph.

3.2. XCT Equivalent Inner and Outer Diameters and Fluctuations Along the Axial Profile Segment

Geometric measurements were performed on consecutive axial sections using the three-point circle fitting method described in Section 2.3.1, and the diameter of the fitted circle in each section was taken as the equivalent inner diameter or equivalent outer diameter of that section. To visually illustrate the slice-by-slice variations in the equivalent inner and outer diameters within the selected axial profile segment, Sample A1 was taken as an example, and its slice-by-slice measurement results are shown in Figure 7. The corresponding curves for the remaining samples are provided in the Supplementary Materials. The horizontal axis represents the slice number within the selected axial profile segment.

Figure 7 shows that the equivalent inner and outer diameters of Sample A1 vary with axial section position and exhibit local peaks and valleys. Each data point in the figure corresponds to a section at a different axial position rather than to repeated measurements of the same section. Therefore, the differences among the data points reflect the slice-to-slice variation in the fitted equivalent diameters across different axial sections under the present measurement conditions.

Based on the slice-by-slice measurements, the mean, standard deviation, minimum, maximum, and range of the equivalent inner and outer diameters of the four models of high-speed ball bearings for new energy vehicles were further calculated. The statistical results are presented in Tables 4 and 5.

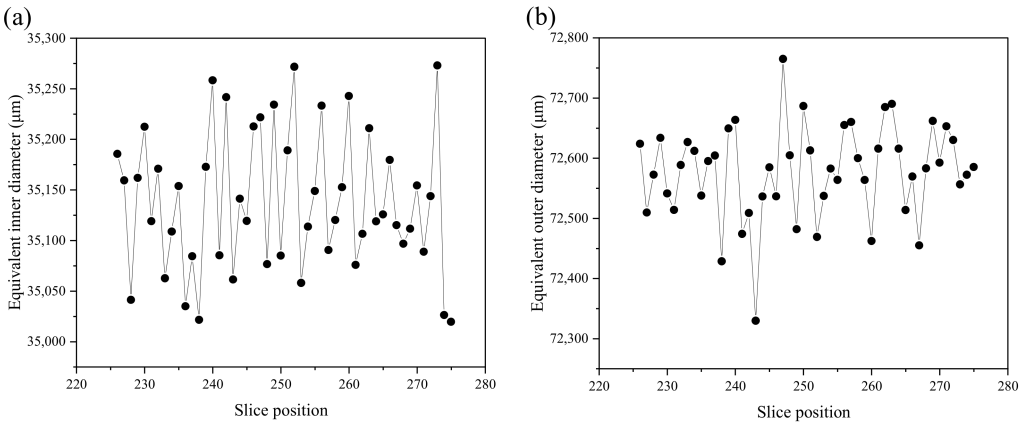


Figure 7. XCT measurements of the equivalent inner and outer diameters of bearing A_1: (**a**) equivalent inner diameter of bearing A_1; (**b**) equivalent outer diameter of bearing A_1.

Table 4. Statistical results of the equivalent inner diameter in the axial profile segment.

Sample No.	Number of Slices	Mean (μm)	Standard Deviation (μm)	Minimum (μm)	Maximum (μm)	Range (μm)
A_1	50	35,137.9	68.6	35,019.5	35,273.1	253.6
A_2	35	34,779.7	76.8	34,607.6	34,968.4	360.8
A_3	20	35,806.7	62.1	35,657.0	35,915.4	258.5
B_1	15	41,287.4	76.4	41,129.2	41,398.6	269.4
B_2	20	40,814.2	86.0	40,651.7	40,968.1	316.4
B_3	30	40,670.6	69.3	40,543.5	40,818.6	275.1
C_1	76	30,274.9	77.4	30,036.6	30,447.0	410.4
C_2	76	31,123.4	84.0	30,927.7	31,315.4	387.7
C_3	20	30,587.8	75.3	30,462.1	30,712.8	250.7
D_1	30	35,090.6	74.4	34,935.1	35,295.3	360.2
D_2	30	35,047.9	54.7	34,938.1	35,155.9	217.7
D_3	25	35,780.2	68.9	35,658.2	35,918.9	260.7

Table 5. Statistical results of the equivalent outer diameter in the axial profile segment.

Sample No.	Number of Slices	Mean (μm)	Standard Deviation (μm)	Minimum (μm)	Maximum (μm)	Range (μm)
A_1	50	72,578.0	78.0	72,329.7	72,765.1	435.4
A_2	35	71,827.4	79.1	71,658.1	72,028.0	369.9
A_3	20	73,846.2	111.3	73,673.8	74,030.6	356.8
B_1	15	82,753.4	104.3	82,587.4	82,908.1	320.7
B_2	20	81,832.6	113.6	81,529.1	82,022.5	493.4
B_3	30	81,529.6	94.0	81,318.3	81,705.1	386.8
C_1	76	72,989.7	98.2	72,599.8	73,252.6	652.8
C_2	76	74,857.8	67.4	74,625.3	74,965.4	340.1
C_3	20	73,621.4	75.8	73,425.2	73,776.1	350.9
D_1	30	80,574.4	72.2	80,412.9	80,735.3	322.4
D_2	30	80,466.1	49.1	80,378.1	80,558.4	180.3
D_3	25	82,072.7	79.1	81,921.1	82,228.0	306.8

Tables 4 and 5 show that, under the present measurement conditions, the equivalent inner and outer diameters of different samples exhibited different degrees of axial variation. Among the samples, B2 had the largest standard deviations for both the equivalent inner

and outer diameters, C1 had the largest ranges for both diameters, whereas D2 had the smallest values for both descriptors. The different behaviors of B2 and C1 with respect to these two statistical descriptors indicate that the standard deviation and range characterize different aspects of axial variation: the standard deviation describes the overall dispersion of the equivalent diameters from consecutive sections around their mean value, whereas the range describes the overall span between the maximum and minimum values. Therefore, both descriptors were used in this study to summarize the degree of axial variation in the equivalent diameters. However, the standard deviation and range can only summarize the overall degree of axial variation and cannot indicate the specific axial positions of local peaks and valleys or their sequence along the axial direction. Such information is preserved in the slice-by-slice equivalent-diameter curves.

3.3. Single-Section Roundness Measurement Results

Based on the cross-sectional profile data obtained using the roundness measuring instrument, the single-section roundness errors of the bore and outer surface of each sample were extracted, as shown in Table 6.

Table 6 shows that the outer-surface roundness errors of the Group D samples were generally higher than those of Groups A–C, whereas the bore roundness errors did not exhibit a consistent variation trend among the different groups. These results indicate differences in the local shape characteristics of the selected sections among the samples.

Table 6. Single-section roundness errors of the bearing bore and outside surface.

Sample No.	Outside-Surface Roundness Error (μm)	Bore Roundness Error (μm)
A_1	1.48	1.51
A_2	1.29	0.40
A_3	1.06	1.66
B_1	1.49	0.63
B_2	0.94	0.77
B_3	0.79	0.98
C_1	0.75	1.03
C_2	0.65	1.51
C_3	1.14	0.97
D_1	2.10	0.85
D_2	2.31	2.02
D_3	1.96	2.91

3.4. Analysis of Deviations Between XCT Measurements and Nominal Dimensions

To compare the XCT measurement results with the nominal dimensions of the bearings, the mean equivalent inner and outer diameters in Tables 4 and 5 were compared with the corresponding nominal dimensions in Table 1, respectively. The absolute deviation and relative deviation were then calculated according to the method described in Section 2.3.1, and the results are shown in Table 7.

Table 7 shows that the relative deviations between the XCT-measured mean equivalent inner and outer diameters and the corresponding nominal dimensions varied among the samples. The relative deviations of A1, A2, D1, and D2 were relatively small, whereas those of B1 and C2 were relatively large. In particular, C2 exhibited the largest relative deviations in both the equivalent inner and outer diameters among all samples. Overall, the magnitude of the differences between the XCT mean equivalent dimensions and the corresponding nominal dimensions was not consistent either among different bearing types or among different samples of the same type.

Table 7. Deviations of XCT measurements relative to nominal dimensions.

Sample No.	Absolute Deviation (μm)		Relative Deviation (%)	
	Inner Diameter	Outer Diameter	Inner Diameter	Outer Diameter
A_1	137.9	578.0	0.39	0.80
A_2	220.3	172.6	0.63	0.24
A_3	806.7	1846.2	2.30	2.56
B_1	1287.4	2753.4	3.22	3.44
B_2	814.2	1832.6	2.04	2.29
B_3	670.6	1529.6	1.68	1.91
C_1	274.9	989.7	0.92	1.37
C_2	1123.4	2857.8	3.74	3.97
C_3	587.8	1621.4	1.96	2.25
D_1	90.6	574.4	0.26	0.72
D_2	47.9	466.1	0.14	0.58
D_3	780.2	2072.7	2.23	2.59

3.5. Vibration Measurement Results

To explore whether the axial geometric variations and dynamic vibration states of the same samples exhibited consistent variation trends, the axial variation descriptors of the equivalent inner and outer diameters obtained in Tables 4 and 5 were compared with the vibration test results of the corresponding samples in Table 8.

Table 8 shows that 7 of the 12 samples did not meet the V3 group requirements, in all cases because the high-frequency vibration velocity exceeded the corresponding limit. Further comparison of the vibration results with the axial variation descriptors in Tables 4 and 5 revealed no stable correspondence between the two types of results within the current sample set. For example, B2 had the largest standard deviations of both the equivalent inner and outer diameters among all samples, yet it met the V3 group requirements. In contrast, D2 had the smallest standard deviations and ranges for both the equivalent inner and outer diameters, while its high-frequency vibration velocity still exceeded the corresponding limit.

Table 8. Vibration test results of the bearing samples.

Sample No.	Vibration Acceleration Level (dB)	Vibration Velocity			V3 Group Evaluation
		Low Frequency (μm/s)	Medium Frequency (μm/s)	High Frequency (μm/s)	
A_1	47	46	32	170	Unqualified
A_2	41	40	32	100	Unqualified
A_3	40	44	30	80	Qualified
B_1	43	60	36	52	Qualified
B_2	43	52	40	54	Qualified
B_3	43	62	34	70	Qualified
C_1	44	80	32	110	Unqualified
C_2	44	90	40	150	Unqualified
C_3	43	70	32	80	Qualified
D_1	42	110	52	160	Unqualified
D_2	45	100	60	102	Unqualified
D_3	44	84	53	190	Unqualified

4. Discussion

The above results indicate that slice-by-slice extraction of equivalent diameters from consecutive XCT sections can preserve continuous geometric information on the bear-

ing bore and outer cylindrical surface as a function of axial position. The slice-by-slice equivalent-diameter curves can reflect the axial positions of local peaks and valleys and their distribution sequence, whereas the mean, standard deviation, and range are used to summarize the overall dimensional level and the degree of axial variation. Thus, the two reflect different aspects of the continuous axial geometric information. In contrast, single-section roundness measurement mainly reflects the local shape characteristics of the selected sectional profile relative to the reference circle. Accordingly, XCT-based continuous axial characterization and single-section roundness measurement are complementary: the former provides continuous variation information across different axial positions, whereas the latter reflects the local profile characteristics of a selected section. Therefore, the primary significance of using XCT in this study is not to demonstrate that its absolute dimensional measurement accuracy is superior to that of conventional precision measurement, but rather to supplement the continuous axial geometric information that is difficult to obtain directly from single-section measurements.

The interpretation of the above axial variations should also take into account the influence of the present measurement conditions. Variations in the fitted equivalent diameters among consecutive sections may arise from geometric differences in the samples themselves and may also be affected by factors such as the effective pixel size of XCT, metal artifacts, boundary grayscale transitions, manual point selection, and scanning and reconstruction geometry. Therefore, the standard deviation and range were used in this study to describe the degree of axial variation in the equivalent inner and outer diameters under the present measurement conditions, rather than directly interpreting these variations as actual manufacturing deviations of the bearings. The differences between the XCT mean equivalent inner and outer diameters and the corresponding nominal dimensions represent only numerical differences between the current measurement results and the nominal dimensions. Because the actual reference dimensions of the individual samples were not obtained through independent high-precision measurements in this study, these differences cannot be directly used to assess the actual manufacturing deviations of the samples or as a basis for evaluating the absolute dimensional accuracy of XCT. Further evaluation of the dimensional measurement accuracy and measurement uncertainty of XCT still requires independent reference measurements, together with repeated scanning, repeated reconstruction, and repeated point-selection tests.

On this basis, the axial geometric variation descriptors obtained by XCT were further compared exploratorily with the vibration test results of the same samples. Within the current sample set, no stable correspondence was observed between the two types of results. The XCT descriptors mainly characterize the axial geometric variations in the bearing bore and outer cylindrical surface, whereas bearing vibration is also influenced by multiple factors, including the surface condition of the raceways, the condition of the rolling elements, assembly clearance, contact stiffness, load, and rotational speed. Therefore, the current results are insufficient to establish a direct causal relationship or predictive model between axial geometric variations and vibration responses. Future studies should increase the sample size under consistent test conditions and further consider the local geometric characteristics of the raceways and rolling elements to more systematically evaluate the relationship between geometric condition and vibration response.

5. Conclusions

In this study, XCT was used to scan and reconstruct three-dimensional models of four types of high-speed ball bearings for new energy vehicles. Based on the reconstruction results, the equivalent inner diameter, equivalent outer diameter, and fluctuations in the equivalent inner and outer diameters within the axial profile segment were analyzed. The

results were also evaluated together with the roundness measurement and vibration test results. The main conclusions are as follows:

(1) XCT can obtain three-dimensional structural information of high-speed ball bearings for new energy vehicles under nondestructive conditions. With appropriate scanning parameter settings and geometric parameter correction, the main bearing structures, including the inner ring, outer ring, and rolling elements, can be displayed relatively clearly, providing a basis for subsequent geometric dimensional measurement and axial profile segment analysis.

(2) The proposed method for characterizing the equivalent inner and outer diameters within an axial profile segment can obtain a sequence of equivalent diameters over a selected axial range from consecutive XCT slices, thereby characterizing axial geometric variations that are difficult to capture using conventional single-section measurements. The mean, standard deviation, and range describe the overall dimensional level and degree of variation, whereas the slice-by-slice equivalent diameter curves preserve the axial positional order and local variation characteristics. Therefore, combining the consecutive axial sequences with statistical parameters enables a more comprehensive characterization of axial geometric variations and complements conventional single-section roundness measurements.

(3) The mean equivalent inner and outer diameters measured by XCT showed different degrees of deviation relative to the corresponding nominal dimensions. The relative deviations of the inner and outer diameters ranged from 0.14% to 3.74% and from 0.24% to 3.97%, respectively. Because the nominal dimensions are not the actual reference dimensions of individual samples obtained by high-precision measurement, these results can only reflect the differences between the XCT measurement means and the nominal dimensions and cannot be directly used to evaluate the absolute dimensional accuracy of XCT. In the vibration tests, 7 samples did not meet the V3 group requirements, and all of these cases were caused by the high-frequency vibration velocity exceeding the limit. The comparison of the vibration results is exploratory. For the current samples, no stable correspondence was observed between the XCT equivalent inner- and outer-diameter fluctuation descriptors used in this study and the vibration levels. Because the dynamic response of bearings is also affected by multiple factors, the present results are insufficient to determine whether a general relationship exists between axial geometric characteristics and vibration responses.

This study still has certain limitations. Because independent high-precision reference measurements and repeated scanning, repeated reconstruction, and repeated point-selection tests have not yet been conducted, the measurement accuracy and measurement uncertainty of XCT dimensional measurements cannot currently be quantitatively evaluated. Therefore, the present study mainly demonstrates the feasibility of this method for the nondestructive characterization of continuous axial geometric variations, while its metrological performance still requires further validation.

Supplementary Materials: The following supporting information can be downloaded at https://www.mdpi.com/article/10.3390/app162110563/s1, Figure S1: Slice-by-slice variations in the equivalent inner and outer diameters of Samples A_2 and A_3; Figure S2: Slice-by-slice variations in the equivalent inner and outer diameters of Group B bearing samples; Figure S3: Slice-by-slice variations in the equivalent inner and outer diameters of Group C bearing samples; Figure S4: Slice-by-slice variations in the equivalent inner and outer diameters of Group D bearing samples.

Author Contributions: Conceptualization, Y.Z. and H.W.; methodology, Y.Z., F.Z. and S.D.; validation, S.J. and S.D.; formal analysis, F.Z. and Y.Z.; investigation, F.Z. and S.J.; resources, S.J.; data curation, F.Z.; writing—original draft preparation, F.Z.; writing—review and editing, Y.Z., S.J., H.W. and J.P.; visualization, F.Z.; supervision, Y.Z. and H.W.; project administration, Y.Z. and H.W. All authors have read and agreed to the published version of the manuscript.

Funding: This research was supported by the Henan Province University-Enterprise Collaborative Innovation Project (No. 26AXQXT027), the Young Talent Support Program of Henan Association for Science and Technology (No. 2025HYTP023), the Henan Province 2025 Integrated Pilot Project for Agricultural Machinery Research, Development, Manufacturing, Promotion, and Application (No. HNYTH2025-01), and the 2026 Outstanding Young Innovative Talents Program of Henan University of Science and Technology (No. 2026HNKJDXYXQNCXRC18).

Institutional Review Board Statement: Not applicable.

Informed Consent Statement: Not applicable.

Data Availability Statement: The original contributions presented in this study are included in the article. Further inquiries can be directed to the corresponding author.

Acknowledgments: The authors would like to thank Kun Zhao (Cixing Group Co., Ltd., Ningbo 315300, China; zhaokun@cwbearing.com.cn) for providing the experimental materials and offering technical guidance during the experiments.

Conflicts of Interest: Songyang Jia is affiliated with Luoyang Bearing Group Co., Ltd.,the other authors declare no conflicts of interest.

References

1. Ministry of Industry and Information Technology of the People's Republic of China. *Regulations on the Access Administration of New Energy Vehicle Manufacturers and Products*; Order No. 39 of the Ministry of Industry and Information Technology of the People's Republic of China; Ministry of Industry and Information Technology of the People's Republic of China: Beijing, China, 2017.
2. López, I.; Ibarra, E.; Matallana, A.; Andreu, J.; Kortabarria, I. Next generation electric drives for HEV/EV propulsion systems: Technology, trends and challenges. *Renew. Sustain. Energy Rev.* **2019**, *114*, 109336. [CrossRef]
3. Lokhande, R.; Mishra, S.K.; Ronanki, D.; Shakya, P.; Edachery, V.; Lijesh, K.P. Review on tribological and vibration aspects in mechanical bearings of electric vehicles: Effect of bearing current, shaft voltage, and electric discharge material spalling current. *Lubricants* **2025**, *13*, 349. [CrossRef]
4. Guo, Q.; Liu, C.; Lv, J.; Liu, S. Friction and Wear Behaviors of PI/MoS2 Bearing Cage Composite Under Elevated Temperature Conditions. *Polymers* **2026**, *18*, 716. [CrossRef]
5. Tohyama, M.; Ohmiya, Y.; Hirose, M.; Matsuyama, H.; Toda, T.; Hasegawa, K.; Onizuka, T.; Sato, H.; Yokoi, M.; Sato, N. Visualization of oil-lubrication ball bearings at high rotational speeds. *Front. Mech. Eng.* **2024**, *10*, 1416656. [CrossRef]
6. Yu, Q. Research and Validation of Cage Design of High Speed Deep Groove Ball Bearings for New Energy Vehicles. *J. Mech. Transm.* **2023**, *47*, 123–130. [CrossRef]
7. Yu, Y.; Chen, G.; Li, J.; Xue, Y. Influence of Geometric Error of Rollers on Rotational Accuracy of Cylindrical Roller Bearings. *J. Northwest. Polytech. Univ.* **2019**, *37*, 774–784. [CrossRef]
8. Shi, J.; Yu, Y.; Jiang, X.; Li, C.; Shen, C.; Huang, W.; Zhu, Z. Dynamic modeling considering time-varying contact pairs and parameterized defects of deep groove ball bearings for its vibration characteristic analysis. *Nonlinear Dyn.* **2024**, *112*, 17781–17809. [CrossRef]
9. Liu, Y.; Li, T.; Hu, P.; Jiang, Y. Nonlinear dynamics analysis of ball bearings subject to varying clearance considering the interference fit. *Nonlinear Dyn.* **2025**, *113*, 30931–30947. [CrossRef]
10. *GB/T 32324-2015*; Rolling Bearings—Methods for the Measurement and Assessment of Departure from Roundness and Waviness. Standardization Administration of the People's Republic of China: Beijing, China, 2016.
11. Bulatov, K.; Chukalina, M.; Buzmakov, A.; Nikolaev, D.; Arlazarov, V.V. Monitored Reconstruction: Computed Tomography as an Anytime Algorithm. *IEEE Access* **2020**, *8*, 110759–110774. [CrossRef]
12. Azmi, B.; Stefanus, M. Investigation of multiphase condition in pipeline using gamma computed tomography. *Ganendra Maj. IPTEK Nukl.* **2019**, *22*, 103. [CrossRef]
13. Schmitt, R.; Niggemann, C. Uncertainty in measurement for x-ray-computed tomography using calibrated work pieces. *Meas. Sci. Technol.* **2010**, *21*, 054008. [CrossRef]
14. Zhao, Y.; Zhou, Y.; Wang, Y.; Wang, N.; Du, Y.; Dong, W.; Zhang, H.; Wang, X.; Xie, H.; Ju, D.; et al. Copper Iodide Ink Scintillator-Based X-Ray Detector for High-Resolution Computed Tomography Imaging. *Laser Photonics Rev.* **2025**, *20*, e02301. [CrossRef]
15. Hampai, D.; Galdenzi, F.; Capitolo, E.; Di Filippo, A.; Dabagov, S.B. X-ray Computed Tomography—From synchrotron to desktop applications. *Nucl. Instrum. Methods Phys. Res. Sect. A Accel. Spectrometers Detect. Assoc. Equip.* **2025**, *1077*, 170544. [CrossRef]
16. Lu, R.; He, P.; Chen, G.; Fang, M. A Review of Computed Laminography Technology: Principle, Artifact Suppression, and Applications. *IEEE Trans. Instrum. Meas.* **2026**, *75*, 1–24. [CrossRef]

17. Wevers, M.; Kerckhofs, G.; Pyka, G.; Herremans, E.; Ende, V.A.; Hendrickx, R.; Verstrynge, E.; Msrien, A.; Valcke, B.; Prreyt, B.; et al. X-ray Computed Tomography for Non-Destructive Testing. In *Proceedings of the 4th International Conference on Industrial Computed Tomography (iCT 2012), Wels, Austria, 19–21 September 2012*; NDT.net: Bad Breisig, Germany, 2012; pp. 13–29.
18. Busch, M.; Hausotte, T. Simulation-based investigation of the metrological interface structural resolution capability of X-ray computed tomography scanners. *J. Sens. Sens. Syst.* **2023**, *12*, 5003824. [CrossRef]
19. Hardner, M.; Liebold, F.; Wagner, F.; Maas, H.G. Investigations into the Geometric Calibration and Systematic Effects of a Micro-CT System. *Sensors* **2024**, *24*, 5139. [CrossRef]
20. Villarraga-Gómez, H.; Herazo, E.L.; Smith, S.T. X-ray computed tomography: From medical imaging to dimensional metrology. *Precis. Eng.* **2019**, *60*, 544–569. [CrossRef]
21. Noda, T.; Shibasaki, K.; Miyata, S.; Taniguchi, M. X-Ray CT Imaging of Grease Behavior in Ball Bearing and Numerical Validation of Multi-Phase Flows Simulation. *Tribol. Online* **2020**, *15*, 36–44. [CrossRef]
22. Kim, J.Y.; Lee, D.H.; Jung, D.H. A Study on Abnormal Detection of High-Speed Bearings for Electric Vehicle Drive Systems. *Int. J. Automot. Technol.* **2024**, *26*, 353–357. [CrossRef]
23. Zi, M.; Ye, J.; Cai, H.; Yang, H.; Chen, G.; Zhang, J.; Li, D.; Lu, D. Experimental Study on Temperature Rise of New Energy Vehicle Drive Motor Bearings Under Grease and Driving Conditions. *Lubricants* **2025**, *13*, 526. [CrossRef]
24. Casaccia, S.; Pandarese, G.; Castorani, V.; Revel, G.M. Design of an experimental approach based on the contrast-to-noise ratio measurement for X-ray computed tomography parameters optimization applied to a carbon fiber-reinforced polymer materials scan. *Acta IMEKO* **2024**, *13*, 1–8. [CrossRef]
25. Reiter, M.; Krumm, M.; Kasperl, S.; Kuhn, C.; Erler, M.; Weiß, D.; Heinzl, C.; Gusenbauer, C.; Kastner, J. Evaluation of transmission based image quality optimisation for X-ray computed tomography. In *Proceedings of the Conference on Industrial Computed Tomography (iCT2012), Wels, Austria, 19–21 September 2012*; Shaker Verlag: Aachen, Germany, 2012; pp. 241–250.
26. *GB/T 32325-2015*; Rolling Bearings—Specifications for Vibration (Velocity) of Deep Groove Ball Bearings. Standardization Administration of the People's Republic of China: Beijing, China, 2016.

Disclaimer/Publisher's Note: The statements, opinions and data contained in all publications are solely those of the individual author(s) and contributor(s) and not of MDPI and/or the editor(s). MDPI and/or the editor(s) disclaim responsibility for any injury to people or property resulting from any ideas, methods, instructions or products referred to in the content.